ARL-TR-10436 ● SEP 2026

Initial Nonlinear Optical Characterization of 2D Layered Materials: Second Harmonic Generation of Monolayer Dichalcogenides

by Frank C. De Lucia Jr. and Nhan C. Dang

NOTICES

Disclaimers

The findings in this report are not to be construed as an official Department of the Army position unless so designated by other authorized documents.

Citation of manufacturer's or trade names does not constitute an official endorsement or approval of the use thereof.

Destroy this report when it is no longer needed. Do not return it to the originator.

ARL-TR-10436 ● SEP 2026

Initial Nonlinear Optical Characterization of 2D Layered Materials: Second Harmonic Generation of Monolayer Dichalcogenides

Frank C. De Lucia Jr. and Nhan C. Dang
DEVCOM Army Research Laboratory

REPORT DOCUMENTATION PAGE

1. REPORT DATE	2. REPORT TYPE	3. DATES COVERED	
		START DATE	END DATE
September 2026	Technical Report	10/1/2025	7/31/2026

4. TITLE AND SUBTITLE
Initial Nonlinear Optical Characterization of 2D Layered Materials: Second Harmonic Generation of Monolayer Dichalcogenides

5a. CONTRACT NUMBER	5b. GRANT NUMBER	5c. PROGRAM ELEMENT NUMBER
5d. PROJECT NUMBER	**5e. TASK NUMBER**	**5f. WORK UNIT NUMBER**

6. AUTHOR(S)
Frank C. De Lucia Jr. and Nhan C. Dang

7. PERFORMING ORGANIZATION NAME(S) AND ADDRESS(ES)	8. PERFORMING ORGANIZATION REPORT NUMBER
DEVCOM Army Research Laboratory ATTN: FCDD-RLA-WA Aberdeen Proving Ground, MD 21005	ARL-TR-10436

9. SPONSORING/MONITORING AGENCY NAME(S) AND ADDRESS(ES)	10. SPONSOR/MONITOR'S ACRONYM(S)	11. SPONSOR/MONITOR'S REPORT NUMBER(S)
Office of the Under Secretary of War and DEVCOM Army Research Laboratory	OUSW, DEVCOM ARL	ARAP-0602251D8Z

12. DISTRIBUTION/AVAILABILITY STATEMENT
DISTRIBUTION STATEMENT A. Approved for public release: distribution unlimited.

13. SUPPLEMENTARY NOTES
ORCIDs: Frank C. De Lucia Jr., 0000-0003-2759-6978; Nhan C. Dang, 0009-0000-5752-8330

14. ABSTRACT
We have measured the nonlinear optical (NLO) responses of 2D layered materials, focusing on second harmonic generation (SHG). Femtosecond laser pulses produced SHG from monolayers of molybdenum disulfide (MoS_2) and tungsten disulfide (WS_2). Both monolayers exhibited strong SHG signals at all four excitation wavelengths tested: 800, 1200, 1300, and 1400 nm. We also observed the expected quadratic relationship between SHG spectrum intensity and laser power. WS_2 produced a stronger SHG signal from 800-nm excitation, whereas SHG from MoS_2 was stronger among 1200, 1300, and 1400 nm. This initial work provides the foundation for further NLO studies including third harmonic generation, polarization/lattice orientation, and optical susceptibility calculations.

15. SUBJECT TERMS
Weapons Sciences, nonlinear optical properties, second harmonic generation, 2D layered materials, ultrafast, transition metal dichalcogenides, graphene

16. SECURITY CLASSIFICATION OF:			17. LIMITATION OF ABSTRACT	18. NUMBER OF PAGES
a. REPORT	b. ABSTRACT	C. THIS PAGE		
UNCLASSIFIED	UNCLASSIFIED	UNCLASSIFIED	UU	20

19a. NAME OF RESPONSIBLE PERSON	19b. PHONE NUMBER *(Include area code)*
Frank C. De Lucia Jr.	(520) 691-5663

STANDARD FORM 298 (REV. 5/2020)
Prescribed by ANSI Std. Z39.18

Contents

List of Figures iv

1. Introduction 1

2. Experimental 2

3. Results 4

4. Conclusions 10

5. References 11

List of Symbols, Abbreviations, and Acronyms 13

Distribution List 14

List of Figures

Figure 1. Experimental setups for (a) 800-nm pump wavelength (b) with OPA. (a: attenuator; hwp: half wave plate; bp1: band-pass filter; fl: 100-mm focusing lens; hs: harmonic separator; 2DLM: 2D layered material; mo: microscope objective; bp2: band-pass filter; spec: spectrometer; iccd: intensified charge-coupled device; lpf: long-pass filter; nd: variable neutral density filters; lpf: long-pass filter; lpdm: long-pass dichroic mirror.) 3

Figure 2. (a) MoS_2 crystal (yellow arrow [2 mm] shows scale of crystal); (b) SHG spectra at various laser powers; (c) depiction of grid and position of each SHG spectra collected (ovals represent estimated laser spot size); and (d) contour map of SHG intensity overlaid with MoS_2 crystal (blue is maximum SHG signal). 5

Figure 3. SHG spectra of graphene and a graphene bilayer. 6

Figure 4. SHG spectra of (a) WS_2 and (b) MoS_2. The ICCD was set to a gain of 20 with a gate of 1 ms and the laser power was 25 mW. The spectra have all been background corrected. Insets: Magnify the peak of the SHG spectra emission; shaded area is the standard deviation. 7

Figure 5. A log-log plot of the amplitudes from a Gaussian fit of each SHG spectrum as a function of excitation laser power for (a) MoS_2 and (b) WS_2. The inset shows an example of the Gaussian fit (black dashed line) of an SHG spectrum (red circles) from WS_2. The linear fit equations are shown for each 2DLM. The slope is ~2 for each, indicating quadratic dependence. 8

Figure 6. SHG spectra of (a) WS_2 and (b) MoS_2 collected using excitation wavelengths of 1200 nm (blue), 1300 nm (green), and 1400 nm (red). The ICCD was set to a gain of 20 with a gate of 10 μs, and the laser power was 25 mW. The spectra have all been background corrected. . 9

1. Introduction

This report covers initial development of nonlinear optical characterization of two-dimensional layered material (2DLM) experiments that support the Classical-Quantum Hybrid Constructs to Advance Weapon Science (CLAWS) program, an Applied Research for Advancement of Science and Technology Priorities award. One of the goals of the CLAWS program is to exploit new types of materials for robust nanoscale photonic/electronic components that ultimately lead to revolutionary imaging/sensing technology. 2DLMs are excellent potential candidates due to their remarkable light-matter interaction properties that enable strong nonlinear optical (NLO) properties[1] allowing photonic functionality, i.e., photon generation, manipulation, transmission, detection, and imaging.[2] Atomically thin 2DLMs allow for miniaturization and advanced nanofabrication to develop novel nanodevices on integrated chip-scale platforms. Thus, high-performance compact electro/optical devices can be realized in a myriad of research disciplines including, but not limited to, optoelectronics, nanophotonics, imaging/detection, energy storage conversion, biomedicine, and ultrafast optical technologies.[3] Interestingly, the very NLO properties that make 2DLMs ideal candidates for advanced device architectures and performance can also be used to elucidate the fundamental properties of 2DLMs. NLO techniques have been used to determine the number of layers, thickness, crystal orientations, strain directions, influence of defects, and fundamental dynamics of phonons and excitons.[3,4]

Second harmonic generation (SHG), a parametric degenerate process, is one of the most fundamental second-order NLO processes.[2,5,6] During SHG, the output signal is emitted and photons are frequency doubled from the input photons, provided the material has a non-centrosymmetric structure.[7,8] In other words, when two photons of the same frequency come together in a material, they combine to form a new doubled output frequency, $\omega_1 + \omega_1 = 2\omega_1 = \omega_2$. The NLO process can be described using the following equation:

$$P = \varepsilon_0\left(X^{(1)}E + X^{(2)}E^2 + \ldots + X^{(n)}E^n\right) \quad (1)$$

where the polarization P is related to the electric field E of the incident light via a power series, ε_0 is the vacuum permittivity, and $X^{(n)}$ is the nth order of susceptibility. When E is low, the relationship between P and E is linear. As E increases, NLO processes can be observed.[5] The second term, $X^{(2)}E^2$, is the second-order susceptibility, and is responsible for the SHG. The intensity of an SHG signal demonstrates quadratic scaling compared to the input photon intensity. Initial commercial applications of the second-order NLO effect involved SHG of lasers using bulk crystals.[2] In order to realize the full range of applications, 2DLMs

have been explored to find materials with large SHG responses. SHG is an excellent method for characterizing the properties of 2DLMs. In addition, the up-conversion of near infrared (NIR) wavelengths to visible wavelengths via the second-order process allows the use of silicon imaging sensors instead of more complex IR cameras.[9,10]

For this initial work supporting the CLAWS program, we interrogated a variety of 2DLMs with high-intensity femtosecond laser pulses to demonstrate the production of SHG. SHG has been observed in several 2D materials including graphene-like materials and transition metal dichalcogenides (TMDs).[11–14] Using our femtosecond laser, we have observed SHG signals in several 2DLMs from different sources, using different substrates, but we will concentrate our findings on two TMDs: MoS_2 and WS_2. These materials have highly efficient light matter interactions and are non-centrosymmetric.[8,14] We will show the SHG emission from the 2DLMs using different laser pulse energies and wavelengths. Furthermore, we will discuss future directions that are built from our initial study.

2. Experimental

Figure 1 shows the experimental setups we used to produce and collect SHG in the 2DLMs. The two configurations are similar—the major difference is that the setup in Figure 1a uses the fundamental 800 nm from a Ti:S femtosecond laser, while the setup in Figure 1b is configured to use a range of wavelengths from an optical parametric amplifier (OPA). In the setup shown in Figure 1a, a 35-fs, 1-kHz, 6-mJ laser pulse is produced by a femtosecond laser system (Coherent Astrella). We attenuated the laser pulse energy using a half waveplate at 800 nm and a thin film polarizer with the angle of incidence set to the Brewster angle (56°). An additional half waveplate is used to control the polarization of the laser pulses. A band-pass filter at 808 nm with a full width at half maximum (FWHM) of 3.1 nm is used to shape the broadband 800-nm laser pulse from the Ti:S laser and further attenuate the laser energy. The laser passes through a 100-mm focal length convex lens, then passes through a harmonic separator that transmits 800 nm and is focused onto the 2DLM. The focusing lens can be moved closer or further from the sample surface via a translation stage to control the beam spot size. Using the attenuator and the focus lens position allows us to carefully control the energy density on the surface of the 2DLM to prevent any damage to the sample. We used a laser beam profiler to measure the beam size at the location of the 2DLM surface. Typically, the spot size is an elliptical shape measuring 680 × 450 μm. When the 808-nm pulse interacts with the 2DLM, SHG is produced at 404 nm and is collected via back reflection. The 404-nm SHG is reflected by the harmonic separator and collected by a microscope objective (10×, 0.28, Plan Apo, Mitutoyo). The microscope

objective is positioned via a translation stage to collect the maximum SHG emission signal. By controlling the energy density at the sample surface separately from the microscope objective focus, we can maximize the signal we collect and eliminate any damage to the sample. The laser power on the surface of the 2DLM is kept under 50 mW to prevent any damage but is usually operated at much lower powers. The SHG passes through a 405-nm band-pass filter with a 10-nm FWHM to further eliminate any residual from the 808-nm pump wavelength. The SHG is then focused onto an optical fiber and delivered to a Czerny–Turner spectrometer and an intensified charge-coupled device (ICCD) configured to collect SHG signals at 404 nm.

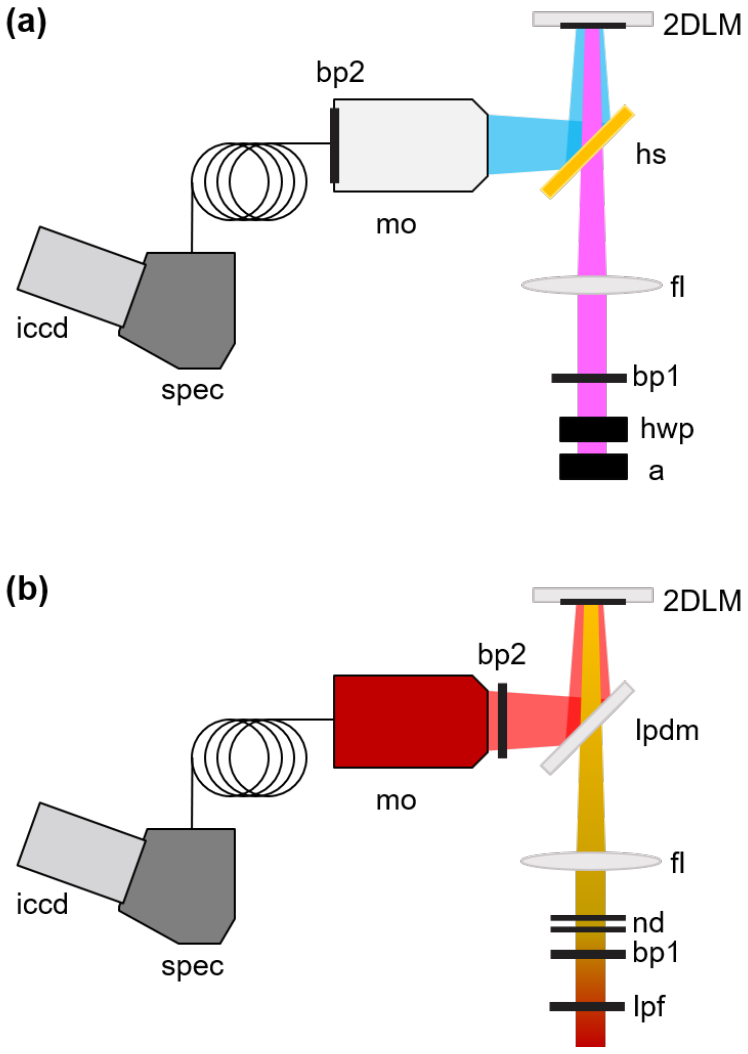

Figure 1. Experimental setups for (a) 800-nm pump wavelength (b) with OPA. (a: attenuator; hwp: half wave plate; bp1: band-pass filter; fl: 100-mm focusing lens; hs: harmonic separator; 2DLM: 2D layered material; mo: microscope objective; bp2: band-pass filter; spec: spectrometer; iccd: intensified charge-coupled device; lpf: long-pass filter; nd: variable neutral density filters; lpf: long-pass filter; lpdm: long-pass dichroic mirror.)

The experimental setup for using the OPA is similar, but instead of an attenuator to control the laser energy, a combination of neutral density filters is used. A long-pass filter with a cutoff wavelength of 900 nm is used to clean up the beam as well. We change the band-pass filter depending on the wavelength used from the OPA; for these initial experiments, the wavelengths are 1200, 1300, and 1400 nm. Instead of a harmonic separator, a long-pass dichroic mirror with a cutoff wavelength of 950 nm is used to allow the NIR wavelength to pass and then reflect the visible SHG wavelength produced upon interaction with the 2DLM. A second band-pass filter is used to block any residual from the pump wavelength. This band-pass filter is matched with the SHG generated from the pump—e.g., a 1300-nm beam would require a 650-nm band-pass filter. The SHG is then collected by a microscope objective (10×, 0.26, Plan Apo NIR, Mitutoyo) and delivered to a spectrometer and ICCD configured to detect SHG signals from 600 to 700 nm.

When we collect a singular SHG emission spectrum, we accumulate 500 SHG spectra on the ICCD from a given sample at one location; this takes several seconds to collect. Then, a background spectrum is collected with the laser blocked under identical conditions and subtracted from the signal. Our initial studies focused on the collection of SHG from a MoS_2 monolayer on quartz, a WS_2 monolayer on quartz, and graphene and graphene bilayers on quartz (2D semiconductors). The samples were all manufactured via chemical vapor deposition and transferred to a 1- ×1-cm quartz substrate. The monolayers are 0.6–0.8 nm thick.

3. Results

Our experiment setup was first tested using a bulk MoS_2 crystal shown in Figure 2a. The incident 800-nm light was translated across the surface until a 400-nm SHG signal was observed. SHG spectra collected at three laser powers are shown in Figure 2b. We then rastered the laser through a grid pattern across the surface and collected SHG spectra at each point on the grid across the MoS_2 crystal (Figure 2c). The maximum intensity at each point was then used to create a contour graph to map the SHG intensity over the entire crystal as shown in Figure 2d. The map shows the heterogeneous nature of the MoS_2 as a function of SHG intensity emission as expected for a bulk sample, since the layered structure will vary considerably.

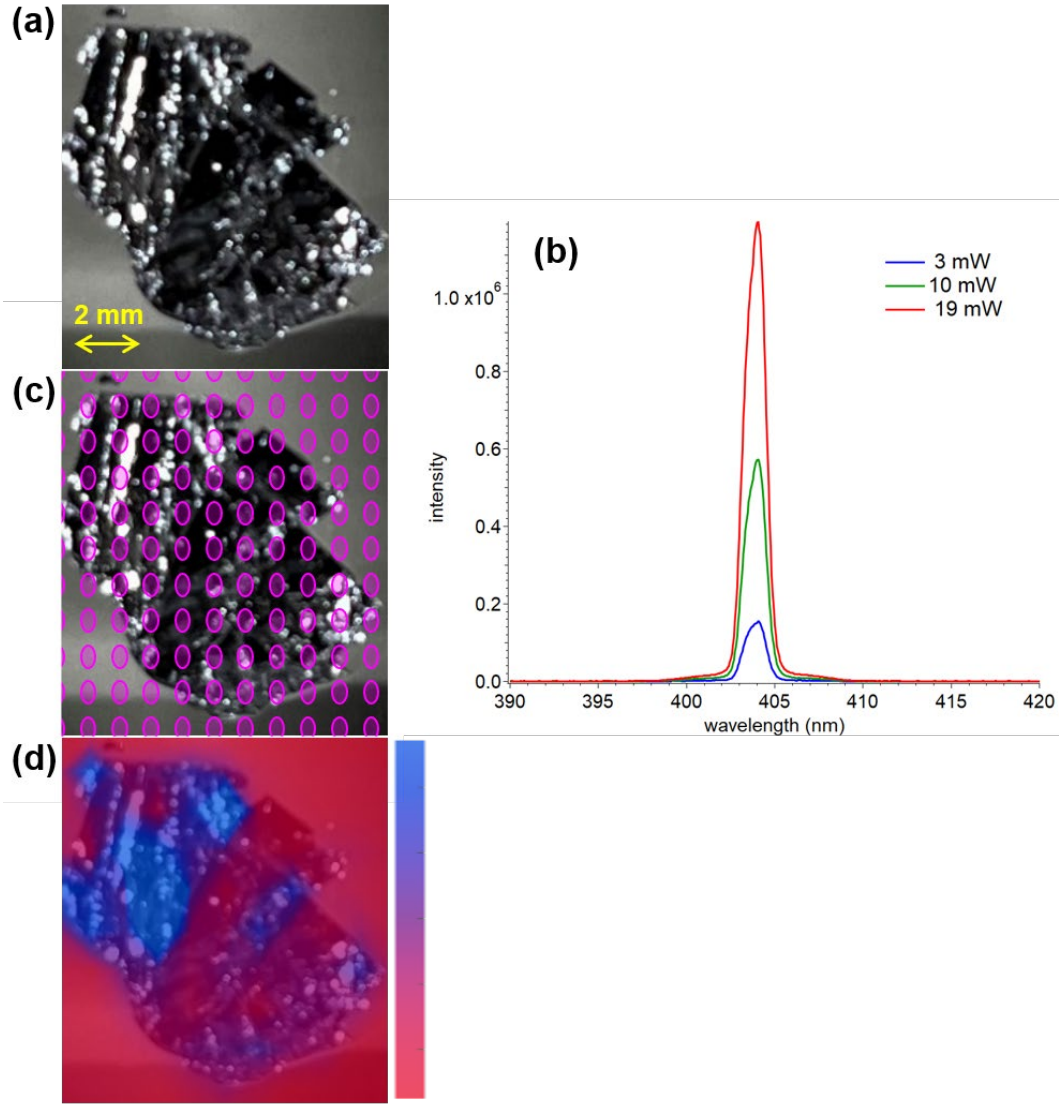

Figure 2. (a) MoS_2 crystal (yellow arrow [2 mm] shows scale of crystal); (b) SHG spectra at various laser powers; (c) depiction of grid and position of each SHG spectra collected (ovals represent estimated laser spot size); and (d) contour map of SHG intensity overlaid with MoS_2 crystal (blue is maximum SHG signal).

Next, we tested a graphene monolayer and a graphene bilayer. As expected, there was no SHG signal from the graphene monolayer due to the centrosymmetric structure of graphene. There were a few areas on the graphene bilayer that had significant emission as seen in Figure 3. These mark areas where the symmetry was disrupted in some way (defects, folds, surface interactions among bilayers, etc.),[2,8,14] thus allowing SHG.

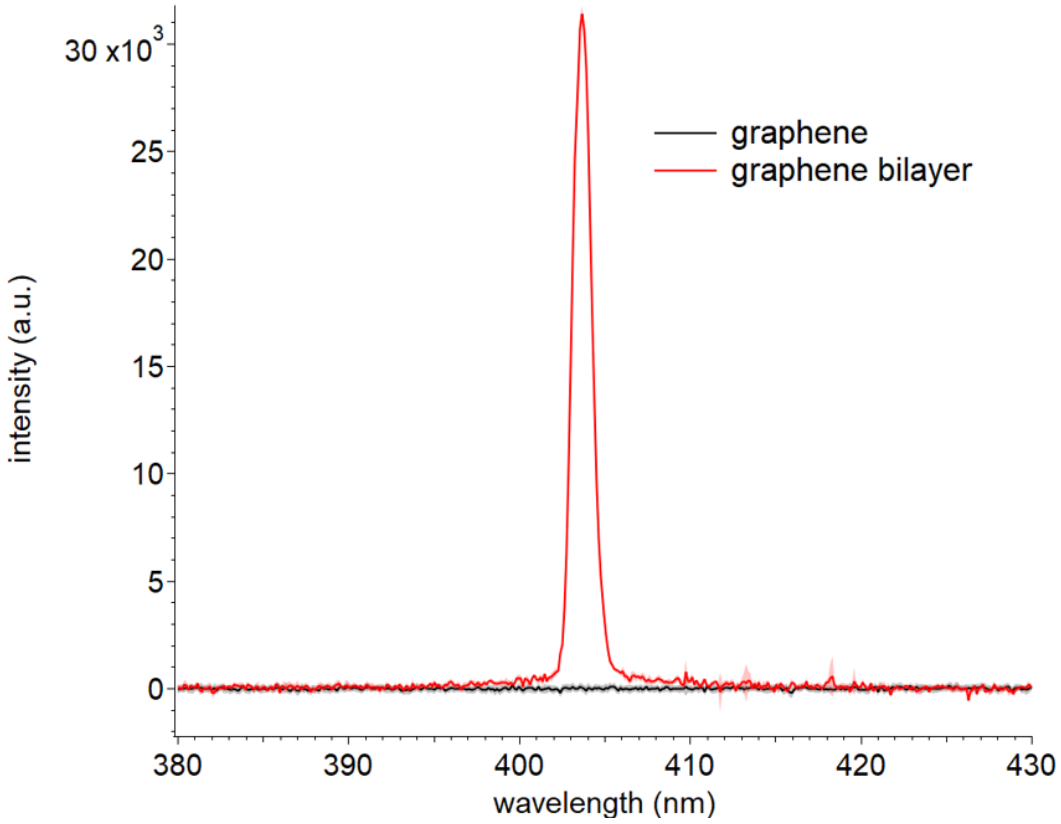

Figure 3. SHG spectra of graphene and a graphene bilayer.

Next, we tested our system against two TMDs: monolayers of WS_2 and MoS_2. In Figure 4, we show SHG spectra of the two monolayers. The WS_2 SHG emission is greater than the MoS_2. Each spectrum in Figure 4 is an average of 10 individual spectra collected from 10 different locations on the 2DLM surface. Five of the spectra were collected on one date and another five were collected at a later date. Compared to the bulk crystal surface, the 2DLM surface SHG intensity variance is less; the WS_2 and MoS_2 relative standard deviation is 3% and 4%, respectively. The insets in Figure 4 emphasize the standard deviation error bars since they are difficult to observe otherwise. This low SHG intensity variance demonstrates the homogeneous nature of the 2DLM samples.

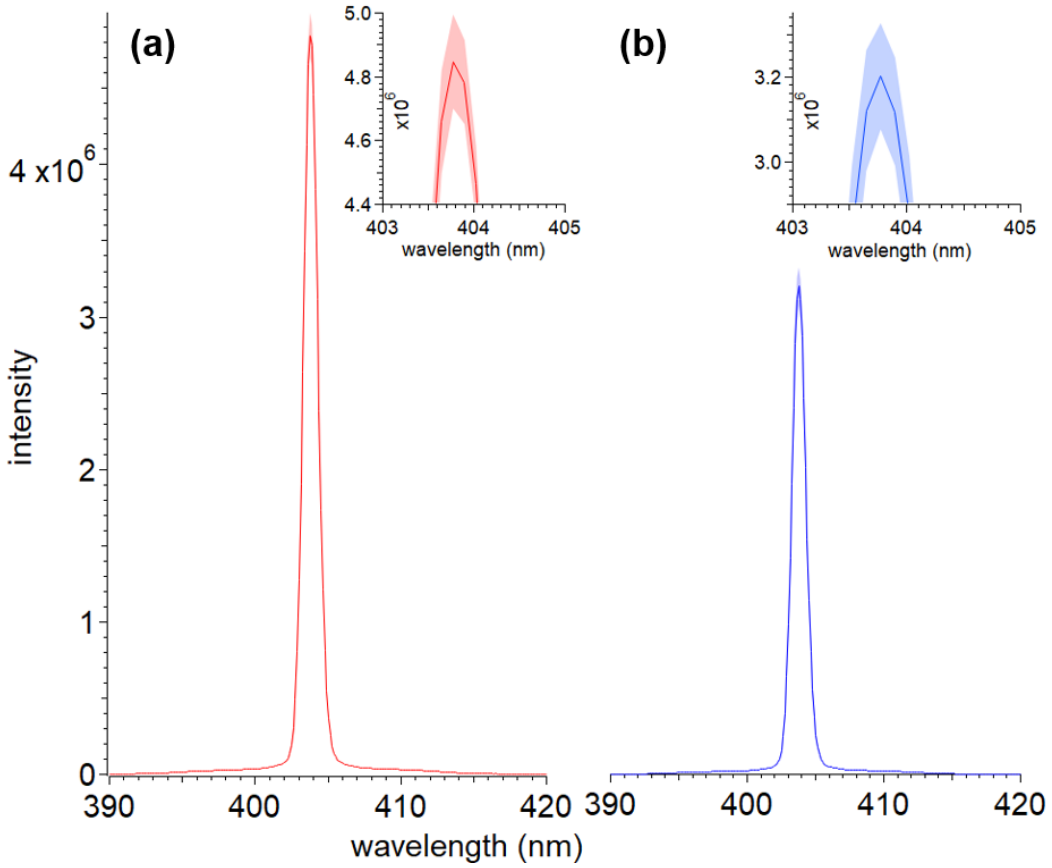

Figure 4. SHG spectra of (a) WS_2 and (b) MoS_2. The ICCD was set to a gain of 20 with a gate of 1 ms and the laser power was 25 mW. The spectra have all been background corrected. Insets: Magnify the peak of the SHG spectra emission; shaded area is the standard deviation.

We collected a series of SHG spectra over a range of laser powers for the 2DLMs. Figure 5 shows the double logarithmic plot of the amplitude of SHG emission relative to excitation laser power for MoS_2 and WS_2. The amplitude of the SHG emission is found by fitting the SHG spectrum to a Gaussian curve. An example fit is shown in the inset of Figure 5. The linear slope is 2.05 ± 0.04 and 2.19 ± 0.05 for MoS_2 and WS_2, respectively, thus following the expected quadratic behavior for relationship between SHG and laser power.[4,6,15–17]

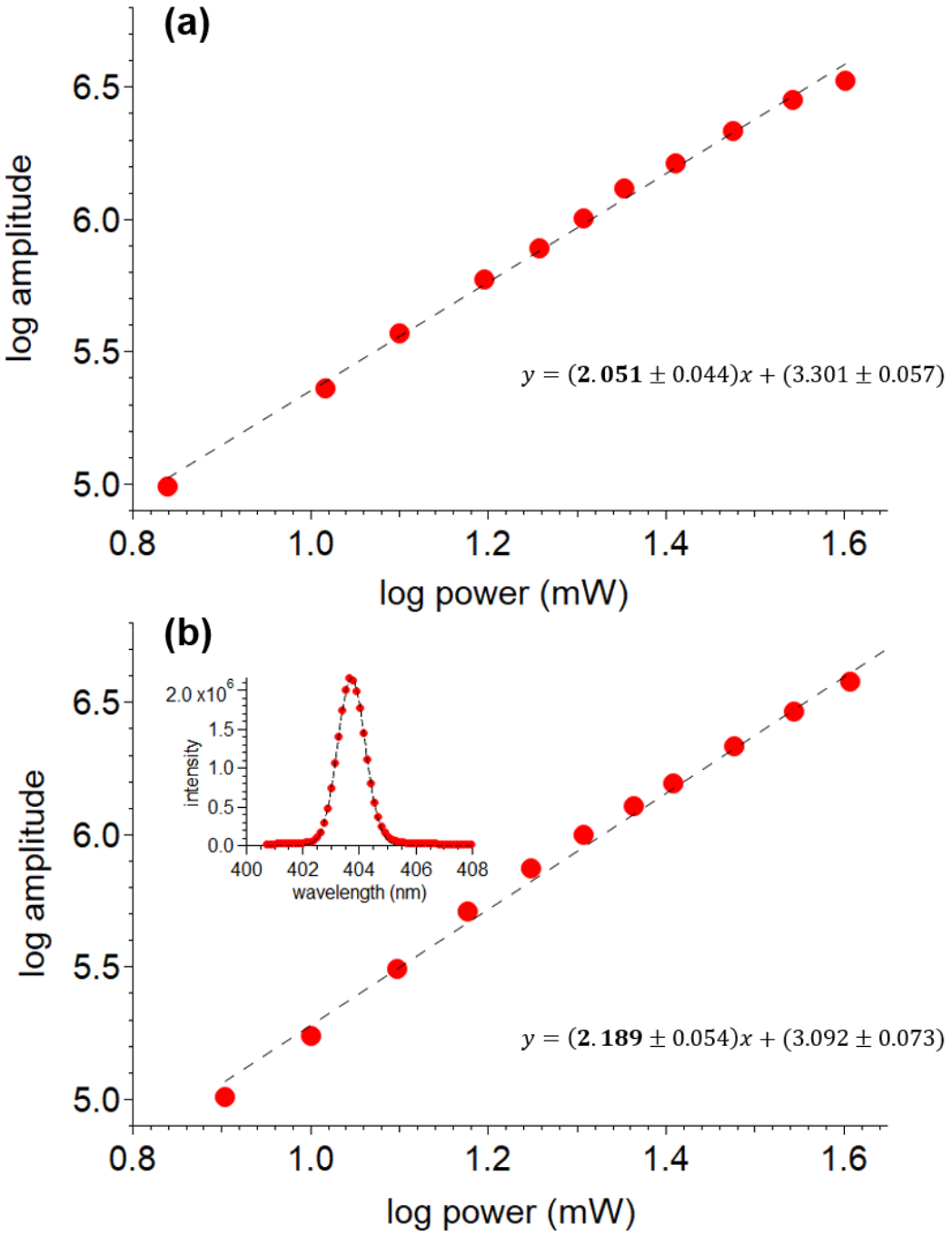

Figure 5. A log-log plot of the amplitudes from a Gaussian fit of each SHG spectrum as a function of excitation laser power for (a) MoS_2 and (b) WS_2. The inset shows an example of the Gaussian fit (black dashed line) of an SHG spectrum (red circles) from WS_2. The linear fit equations are shown for each 2DLM. The slope is ~2 for each, indicating quadratic dependence.

We are also interested in collecting SHG from NIR excitation wavelengths. We used an OPA to provide excitation laser wavelengths at 1200, 1300, and 1400 nm. We collected four individual SHG spectra at four different locations on the monolayers at each wavelength and averaged them for both WS_2 and MoS_2. The SHG spectra for WS_2 (left) and MoS_2 (right) are shown in Figure 6. There is minimal variance from these SHG spectra at each wavelength. The relative standard deviations at the peak of the SHG from WS_2 at 1200, 1300, and 1400 nm are 1.7%, 2.6%, and 3.4%, respectively. The relative standard deviations at the peak of the MoS_2 at 1200, 1300, and 1400 nm are 1.4%, 1.2%, and 1.6%, respectively. The two monolayers follow the same SHG intensity trend, 650 > 600 > 700 nm. However, the MoS_2 SHG intensity is larger at each wavelength compared to WS_2 contrasting with the SHG at 800 nm in Figure 4, where the WS_2 SHG intensity is greater.

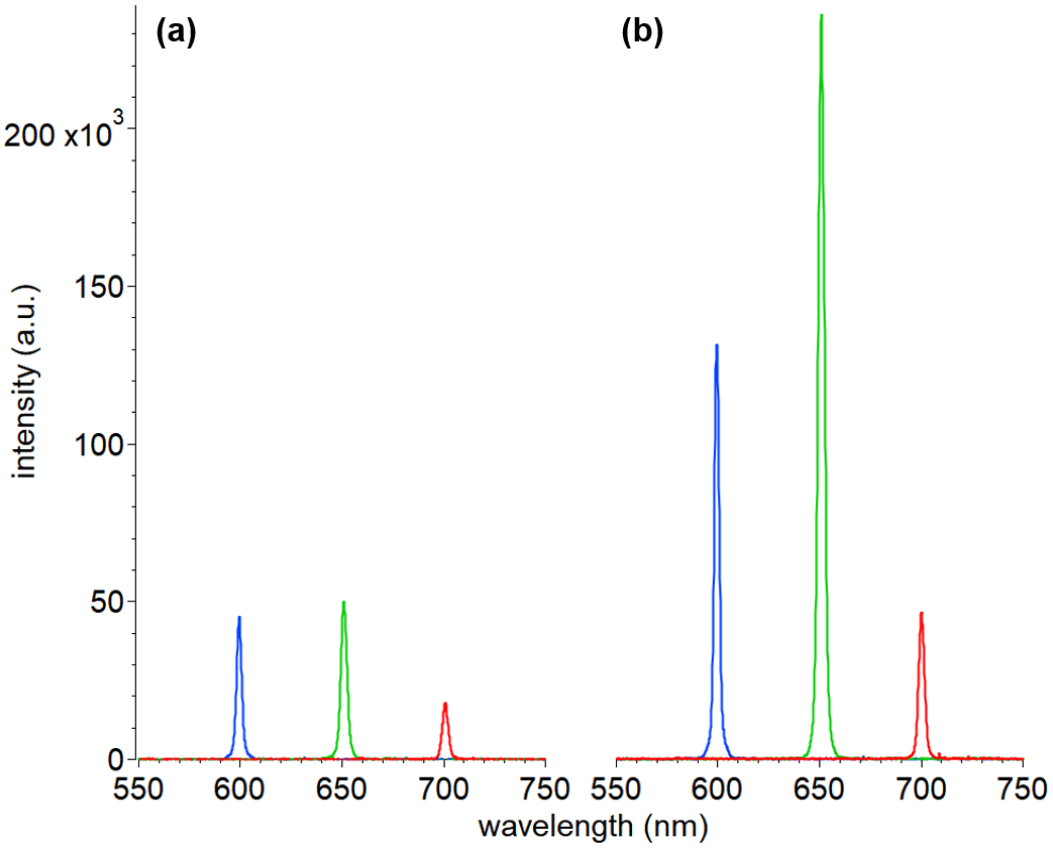

Figure 6. SHG spectra of (a) WS_2 and (b) MoS_2 collected using excitation wavelengths of 1200 nm (blue), 1300 nm (green), and 1400 nm (red). The ICCD was set to a gain of 20 with a gate of 10 µs, and the laser power was 25 mW. The spectra have all been background corrected.

4. Conclusions

We designed and tested an optical setup using a femtosecond laser to measure the NLO effects, specifically SHG, from 2DLMs. This is an initial experiment to show the capabilities that have been developed. We can collect SHG spectra from a variety of 2DLMs using an 800-nm excitation laser as well as a range of wavelengths in the NIR due to the tunability of an OPA. In this work, we showed the SHG spectra collected from WS_2 and MoS_2. We also showed how the SHG intensity dependence on excitation laser power follows the expected quadratic behavior.

There are several planned future directions for our NLO studies. First, we will investigate the third harmonic generation (THG) from 2DLMs. THG is not dependent on crystal symmetry, meaning THG can be observed in 2DLMs such as graphene that have symmetries that forbid SHG emission.[17] THG has potential applications in several types of photonic/imaging devices.[18–20] Next, we want to explore the polarization dependence of SHG since it has been demonstrated that SHG emission is dependent on polarization of the excitation laser relative to the crystal orientation in non-inverse symmetric 2DLMs.[12,13,17,21] This will allow us to use the SHG polarization to characterize the crystal structure in 2DLMs of interest. SHG and THG can also be used to measure optical susceptibilities, $\chi^{(2)}$ and $\chi^{(3)}$. Optical susceptibility determines the strength of nonlinear optical processes; thus, it is an essential parameter to quantify for the development of new types of photonic devices.[6,15,16] We can also explore the effect of device construction, either by using multiple layers of the same 2DLM or hetero materials such as bilayers made of different 2DLMs to investigate any enhancements to optical susceptibilities. Finally, we want to implement a proof-of-concept experiment that will utilize the SHG up-conversion process, i.e., converting IR wavelengths to visible wavelengths, in order to image IR emissions onto less complex silicon devices.

5. References

1. Dogadov O, Trovatello C, Yao B, Soavi G, Cerullo G. Parametric nonlinear optics with layered materials and related heterostructures. Laser Photonics Rev. 2022;16(9):2100726. https://doi.org/10.1002/lpor.202100726

2. Zhang J, Zhao W, Yu P, Yang G, Liu Z. Second harmonic generation in 2D layered materials. 2D Mater. 2020;7(4):042002. https://doi.org/10.1088/2053-1583/abaf68

3. Zhou L et al. Nonlinear optical characterization of 2D materials. Nanomaterials. 2020;10(11):2263. https://doi.org/10.3390/nano10112263

4. Hernandez-Rueda J, Noordam ML, Komen I, Kuipers L. Nonlinear optical response of a WS_2 monolayer at room temperature upon multicolor laser excitation. ACS Photonics. 2021;8(2):550–556. https://doi.org/10.1021/acsphotonics.0c01567

5. Franken PA, Hill AE, Peters CW, Weinreich G. Generation of optical harmonics. Phys Rev Lett. 1961;7(4):118–119. https://doi.org/10.1103/PhysRevLett.7.118

6. Kim S et al. Second-harmonic generation in multilayer hexagonal boron nitride flakes. Opt Lett. 2019;44(23):5792–5795. https://doi.org/10.1364/OL.44.005792

7. Yu S, Wu X, Wang Y, Guo X, Tong L. 2D materials for optical modulation: challenges and opportunities. Adv Mater. 2017;29(14):1606128. https://doi.org/10.1002/adma.201606128

8. Autere A et al. Nonlinear optics with 2d layered materials. Adv Mater. 2018;30(24):1705963. https://doi.org/10.1002/adma.201705963

9. Konkada Manattayil J et al. 2D material based nonlinear optical mirror for widefield up-conversion imaging from near infrared to visible wavelengths. Laser Photonics Rev. 2024;18(10):2400374. https://doi.org/10.1002/lpor.202400374

10. Valencia Molina L et al. Enhanced infrared vision by nonlinear up-conversion in nonlocal metasurfaces. Adv Mater. 2024;36(31):2402777. https://doi.org/10.1002/adma.202402777

11. Seyler KL et al. Electrical control of second-harmonic generation in a WSe_2 monolayer transistor. Nat Nanotechnol. 2015;10(5):407–411. https://doi.org/10.1038/nnano.2015.73

12. Malard LM, Alencar TV, Barboza APM, Mak KF, de Paula AM. Observation of intense second harmonic generation from MoS_2 atomic crystals. Phys Rev B. 2013;87(20):201401–201401. https://doi.org/10.1103/PhysRevB.87.201401

13. Li Y et al. Probing symmetry properties of few-layer MoS_2 and h-BN by optical second-harmonic generation. Nano Lett. 2013;13(7):3329–3333. https://doi.org/10.1021/nl401561r

14. Dean JJ, van Driel HM. Second harmonic generation from graphene and graphitic films. Appl Phys Lett. 2009;95(26):261910–261911. https://doi.org/10.1063/1.3275740

15. Rosa HG et al. Characterization of the second- and third-harmonic optical susceptibilities of atomically thin tungsten diselenide. Sci Rep. 2018;8(1):10035. https://doi.org/10.1038/s41598-018-28374-1

16. Woodward RI et al. Characterization of the second- and third-order nonlinear optical susceptibilities of monolayer MoS_2 using multiphoton microscopy. 2D Materials. 2016;4(1):011006. https://doi.org/10.1088/2053-1583/4/1/011006

17. Khan AR et al. Optical harmonic generation in 2D materials. Adv Funct Materi. 2021;32(3):2105259. https://doi.org/10.1002/adfm.202105259

18. Barad Y, Eisenberg H, Horowitz M, Silberberg Y. Nonlinear scanning laser microscopy by third harmonic generation. Appl Phys Lett. 1997;70(8):922–924. https://doi.org/10.1063/1.118442

19. Weigelin B, Bakker GJ, Friedl P. Third harmonic generation microscopy of cells and tissue organization. J Cell Sci. 2016;129(2):245–255. https://doi.org/10.1242/jcs.152272

20. Jia L et al. Third-order optical nonlinearities of 2D materials at telecommunications wavelengths. Micromachines. 2023;14(2):307. https://doi.org/10.3390/mi14020307

21. Kumar N et al. Second harmonic microscopy of monolayer MoS_2. Phys Rev B. 2013;87(16):161403–161401. https://doi.org/10.1103/PhysRevB.87.161403

List of Symbols, Abbreviations, and Acronyms

2DLM	Two-Dimensional Layered Material
ARAP	Applied Research for Advancement of Science and Technology Priorities
CLAWS	Classical-Quantum Hybrid Constructs to Advance Weapon Science
FWHM	Full Width at Half Maximum
ICCD	Intensified Charge-Coupled Device
IR	Infrared
MoS_2	Molybdenum Disulfide
NIR	Near Infrared
NLO	Nonlinear Optical
OPA	Optical Parametric Amplifier
SHG	Second Harmonic Generation
THG	Third Harmonic Generation
TMD	Transition Metal Dichalcogenide
WS_2	Tungsten Disulfide

1 (PDF)	DEFENSE TECHNICAL INFORMATION CTR DTIC OCA
1 (PDF)	DEVCOM ARL FCDD RLB CB TECH LIB